On the chemical composition, microstructure and mechanical properties of a Nitrogen-contaminated Ti-6Al-4V component built by Wire-Arc Additive Manufacturing

D Hu[1]*, R Biswal[2], V K Sahu[1,3], J W Fellowes[4], A Zadehkabir[2], S W Williams[2] and A E Davis[1]

[1] Department of Materials, The University of Manchester, Manchester, M13 9PL, UK
[2] Welding and Additive Manufacturing Centre, Cranfield University, Bedfordshire, MK43 0PL, UK
[3] Now at Mechanical Engineering, University of North Texas, Denton, 76201, US
[4] Department of Earth and Environmental Sciences, The University of Manchester, M13 9PL, UK

*E-mail: dongchen.hu@manchester.ac.uk

Abstract. Additive manufacturing (AM) using recycled Ti-6Al-4V (Ti64) feedstock material from wrought waste streams is a novel process that can reduce the overall energy cost and carbon (CO_2) footprint when compared to primary-production routes. The potential contamination of recycled feedstock material (e.g. C, O, N and Fe) can affect the microstructure and mechanical properties of the component. In this work, a Ti64 test wall built using wire arc AM (WAAM) was studied, where the top half only was contaminated by N through the shielding gas during deposition. This allowed a direct comparison of Ti64 WAAM material with high and low N content, deposited under otherwise identical conditions, to replicate the worst-case scenario of N contamination from using recycled swarf. The hardness of the N-contaminated section was found to be 25% higher than the uncontaminated section of the wall, demonstrating the N solid solution strengthening in Ti64. The room temperature transformed microstructure was found to have a 25% coarser α-lath thickness, which was proposed to be an effect of the AM cyclical heating and increasing of the β-transus temperature due to a higher level of N. Additionally, the outer layer of the N-contaminated sample section was found to have a refined parent β grain structure.

1. Introduction

Titanium alloys are embraced in the aerospace industry due to their high specific strength, fracture resistance and corrosion resistance [1, 2]. Additive Manufacturing (AM) methods have the advantages of high material utilisation, flexibility for complex shapes and the ability to manufacture near net-shape components [3, 4]. Wire-Arc Additive Manufacturing [4] (WAAM) is one suitable method for fabricating large-scale parts with 'kg/h' high deposition rates, which makes them suitable for production of large aerospace components [5].

A high level of material is wasted in conventional wrought processes during machining [5]. Recycling and reusing the swarf as feedstock materials for AM processes can reduce energy consumption and CO_2 emissions. However, using recycled Ti can introduce contaminant elements like C, N, O and Fe. N is an α-stabilisers [2], which means that a higher level of N could affect the transformation microstructure of an AM as-built component, especially if the contaminant distribution is not homogeneous. However, it is inherently challenging to detect the presence of

Content from this work may be used under the terms of the Creative Commons Attribution 4.0 licence. Any further distribution of this work must maintain attribution to the author(s) and the title of the work, journal citation and DOI.
Published under licence by IOP Publishing Ltd

light elements (like O and N) in Ti microstructures, and the metallurgical effects of N in particular are rarely studied [6]. To accelerate the adoption of recycled Ti into AM aerospace component production, it is important to evaluate the effect of N contamination in Ti64 (and indeed other potential contaminants) on microstructure and resulting mechanical properties, to highlight potential risks for safety-critical parts.

In this study, a Ti64 test WAAM wall was built, with the top half contaminated by N, to directly compare the influence of N on the macro and microstructure. Multiple chemical analyses were conducted to characterise the chemical distribution and microstructure, to discern the metallurgical effects of N contamination in WAAM Ti64.

2. Materials and experiments

A WAAM wall specimen was produced using a 1.2 mm diameter Ti64 wire (wire feed speed: 2.5m/min) with an EWM® Plasma Torch with a travel speed of 5 mm/s. The deposition was performed over a 6.3 mm thick hot rolled Ti64 substrate. A local shielding device with Pureshield® Argon was used to maintain the inert atmosphere around the melt pool during the deposition process. The inert atmosphere was maintained until the temperature of the solidified melt pool dropped to 500°C, as it can be assumed that below this temperature the O_2 and N_2 ingress into Ti64 is negligible. Any changes made in the gas composition supplied to the local shielding device can directly impact the quality of deposition. Therefore, the first 15 layers were deposited using the Pureshield Argon and followed by another 20 layers with a controlled amount of N_2 being added to the local shielding gas mixture. The volumetric ratio of the N_2 to Pureshield Argon was estimated to be 0.11. Since the local shielding device consists of multiple honeycomb flow channels to establish a laminar flow, this also helps in homogenising the gas mixture. The reference frame for the images relative to the WAAM build is defined as: heat source travel direction parallel to the wall or 'welding' direction as WD, the transverse direction as TD and, build height direction normal to each layer as ND (see figure 1a). After deposition, the WAAM wall was removed from the substrate, and several ND-TD cross sections were cut and polished to a 0.04 micron OPS finish.

One ND-TD cross section covering the uncontaminated/contaminated interface region was etched with Kroll's reagent and then a Zeiss AxioCam was used to produce large area stitched optical micrographs. Scanning Electron Microscopy (SEM)-Backscattered Electron (BSE) images were acquired using an FEI Magellan Field Emission Gun (FEG)-SEM to investigate the transformation microstructure. Micro-hardness mapping was performed on another cross section using a Struers Durascan 80 hardness tester. Large area Electron Backscattered Diffraction (EBSD) mapping of both cross sections was performed on a Thermo-Fisher Apreo FEG-SEM equipped with an Oxford Instrument 'Symmetry 2' EBSD detector, operating at an accelerating voltage of 20kV. The EBSD data was further analysed using commercial software AZtecCrystal provided by Oxford Instruments. The β-phase solidification microstructure was reconstructed based on the Burgers orientation relationship between the parent β phase and the transformation α using the parent grain reconstruction capability in AZtecCrystal. A novel Electron Probe Microanalysis with Soft X-ray Emission Spectroscopy (EPMA-SXES) technique was employed to obtain the spatial distribution and quantified concentration of C, N and O, since the characteristic peaks of these light elements are extremely difficult to resolve reliably in a conventional SEM-EDS X-ray spectrum. A more detailed description of the technique will be included in a future publication.

3. Results

The hardness profile shown in figure 1(a) was obtained from micro-hardness mapping by averaging 25 indents in TD, which indicates a significant increase in hardness in the contaminated part (top, ~445HV) than the clean part (bottom, ~ 354 HV). A large area optical image of the etched cross section is presented in figure 1(b), and reveals that the dissimilar-colour interface between the uncontaminated Ti64 material (referred to as 'clean part') and the first contaminated layer (black arrows) is not flat, but instead curved, matching the bead profile of similar Ti64 WAAM deposits in this plane [7]. HAZ bands are also clear in figure 1(b). However, the HAZ bands adjacent to the interface are curved and irregular (red arrows), unlike the parallel HAZ bands in the clean bottom part and those in the top contaminated part but located farther from the interface (orange arrows). The β-reconstructed EBSD map in figure 1(c) shows clear grain refinement in the outer layer of the contaminated part, which differs from the highly textured (<001>//ND) coarse columnar β within the central region and the bottom clean part of the wall. figure 1(d) is a quantified EPMA map showing the N level across the interface. The concentration of N across the interface changes with a stepped profile with a sharp transition between 0.03 wt.% and 0.67 wt.% followed by a gradual gradient, with a final discontinuous transition to ~ 1.1 wt.%, matching the bead profile of several deposited layers. This 'transition gradient' is similar to those seen in WAAM dissimilar-alloy builds where the alloy feedstock is switched mid-deposition [8]. Averaged N concentrations measured by EPMA in the clean/contaminated sections are given in table 1. Similar analysis has also been applied to C and O but show a uniform distribution throughout the deposition.

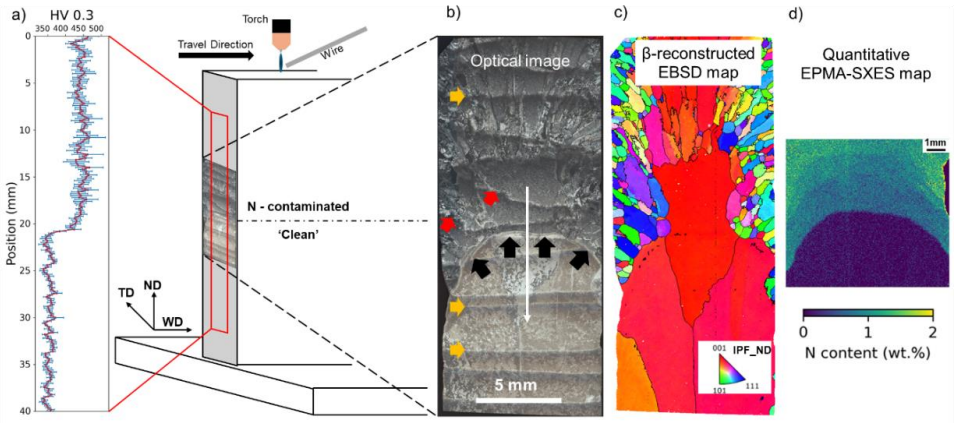


Figure 1. (a) N-contamination WAAM wall schematic diagram and reference frame, alongside a hardness profile on the ND across the interface. (b) An optical image taken from the interface. Fusion boundary between clean and contaminated part is indicated by black arrows. Some HAZ bands are highlighted by red and orange arrows. (c) A β-reconstructed EBSD map of the same area. (d) Quantified EPMA-SXES map showing N level at the interface. The white line on the optical image indicates where the SEM-BSE scanning was performed (figure 2).

The bulk chemical compositions of the contaminated and clean parts were analysed by Inductive Coupled Plasma mass spectroscopy (ICP), and the results are presented in table 1. The ICP results revealed that the top part is only contaminated with N without any significant changes in the level of other elements. Although a bulk concentration of ~0.8 wt.% N was recorded, the unusually high level in the sample was unfortunately outside the instrument calibration range and so can only be considered an estimate. The concentrations of other elements were well within calibration ranges and are therefore considered much more reliable.

Overall, the transformation microstructure consisted of typical α + β basketweave lamellae [7]. Inter-lamellar spacing (ILS) measurements were performed across the contamination interface using the method described by Zhao et al. [9]. ILS measurement was only performed on a single line to avoid the effect of the irregular (non-flat) HAZ bands adjacent to the interface in TD. Across

Table 1. ICP measurement of bulk sample compositions in wt.% taken from the contaminated top and clean bottom of the WAAM wall. * 0.805 wt.% is outside the calibration of the ICP measurement, and can only be taken as an estimate.

Element	Al	V	Fe	C	H	O	N (ICP)	N (EPMA)
Contaminated	6.34	3.83	0.18	0.023	0.0015	0.17	0.805*	1.18
Clean	6.24	3.86	0.17	0.023	0.0011	0.17	0.013	0.03

the HAZ bands a characteristic 'saw tooth', repeating pattern is observed, where the ILS increases as it approaches the bottom of the HAZ band and subsequently drops rapidly at the top of the HAZ band [7]. The abrupt change in ILS is linked to the effect of the α→β phase transformation on transformation microstructure as shown in figure 2, which is consistent with previous work [7].

More importantly, the ILS measurements show that the average ILS is ~25% larger in the contaminated part compared to the clean part. This discrepancy suggests that a higher level of N has a more pronounced effect than the heat accumulation on the α-lath coarsening.

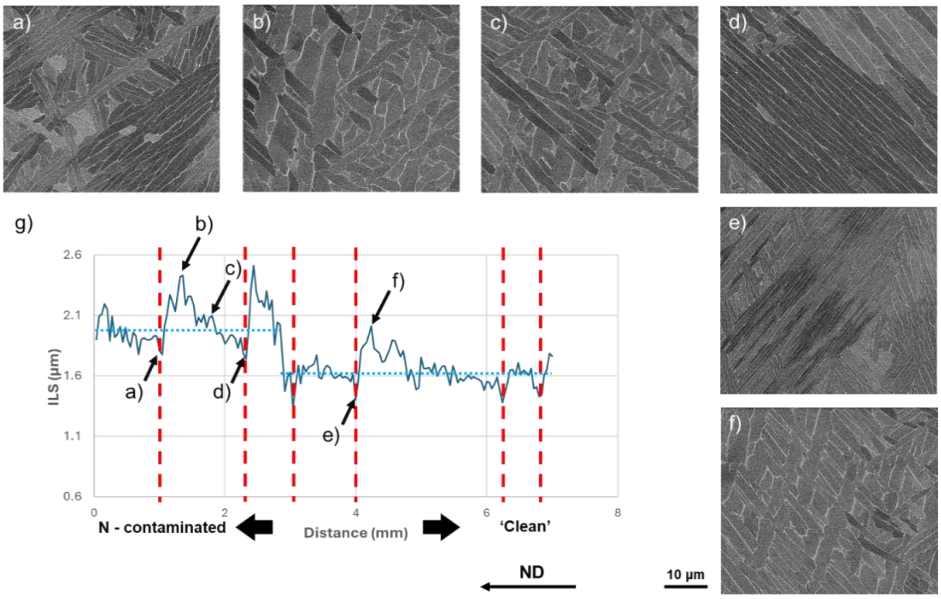


Figure 2. (a-d) Sequential SEM-BSE images showing the microstructure from one HAZ band to another. (e) and (f) are two SEM-BSE images showing the microstructure across one HAZ band from the clean section. (g) Linear intercept α-lamellar spacing (ILS) measurement across 6 HAZ bands across the interface taken from the position highlighted in figure 1(b) by the white arrow.

4. Discussion

The hardness measurement showed that there is a ~25% increase in the contaminated part compared to the clean part, which is indicative of an increase in the yield strength as has been demonstrated previously (e.g. [10]). This increase in hardness is likely attributed to N solid solute strengthening effect, as previously reported in pure Ti [11, 12] but conversely reduces the ductility.

The transformation microstructure analysis reveals a ~25% coarsening of the lath thickness in the contaminated part. Coarsening of the transformation microstructure of Ti64 leads to a higher ductility [13], which could cause the WAAM-built Ti64 component to exhibit an increased

strength without compromising the ductility drastically. O was found to have a similar effect by Caballero [14], where a 0.25% addition of O demonstrated an increase in the strength while retaining similar ductility in uniaxial tensile tests, which could be linked to transformation microstructure coarsening. This could be an advantage of AM processing over conventional casting/wrought processing, due to the high cooling rate that produces a very fine as-built transformation microstructure that can tolerate such coarsening and maintain beneficial mechanical properties.

Nitrogen is an α stabiliser in Ti [2] and is known to have a similar effect as O in increasing the β-transus temperature (T_β) [15]. This is an important consideration in AM Ti64 microstructures with variable N concentration because of the thermal cycling that occurs below the T_β causing partial α→β phase transformation, leading to the formation of HAZ bands. In order to predict the effect of N on the T_β in Ti64, phase transformation temperature calculations of Ti64 were performed using the 'Thermo-calc' software with the ICP measured composition of the contaminated wall, except for the N where the averaged EPMA value (1.18 wt.%) was used that was considered more reliable (see figure 3a). The significant increase in the T_β may explain the coarsening of the transformation microstructure on the N-contaminated side. During the thermal cycling below T_β, the α regions are subjected to partial α→β phase transformation leading to transformation microstructure coarsening [7]. A higher N content in the contaminated section is proposed to accelerate this coarsening kinetic as the partial phase transformation occurs at a higher temperature and leads to a coarser transformation microstructure than in the clean section.

However, the spatial distribution of N, as revealed by the EPMA map in figure 3(d), is heterogeneous along the TD. The EPMA map shows a sharp N gradient directed towards the 'C' shaped interface, which is consistent with the bead profile. As illustrated by the N profile along the ND in figure 3(b), there is a sharp transition at the interface followed by a gradual gradient which results from the remelting and liquid mixing of the previous layer during deposition. After depositing another 2 layers above the interface (approximately 4 mm), the N content reaches a steady level. Figure 3(c) is a schematical illustration of the N spatial distribution of a ND-TD cross section. Red, yellow and green dashed lines along the TD were plotted on figure 3(c) to represent locations that experienced the same thermal history and align with the HAZ bands at the build centreline. Corresponding T_β schematic profiles (based on the N EPMA map and phase diagram trends) that match the same centreline positions have been added in figure 3(d) and are proposed to correspond to the curvature of the irregular HAZ bands shown in figure 1(b). Initially, there is a high N gradient when crossing the fusion boundary (that is aligned with the bead profile) in TD between layers, which results in high HAZ band curvature. However, as the N gradient diminishes moving further from the interface, the curvature of the T_β profile and HAZ bands decrease.

Furthermore, the outer layer of the N-contaminated section was found to have a refined parent β grain structure as illustrated in figure 1(c). This observation is consistent with previous findings in dual phase Ti alloys with wider mushy zones [8]. It is suggested that the outer layer refinement is caused by the maximum thermal gradient tilting away from the ND during solidification, following the normal of the curved bead profile. This allows the dendrites growing away from the ND to gain a growth advantage over the <001> // ND columnar β grains and block their growth. This effect is explained in more detail in reference [16]. The thermal gradient is more likely to affect the N contaminated section, since N is known to increase the width of the mushy zone. In addition, due to the relatively high level of N in the sample, nitrides may form in the melt pool, which could act as heterogeneous nucleation sites and contribute to the β grain refinement during solidification, which has been demonstrated with artificial nucleants introduced to the melt pool [17].

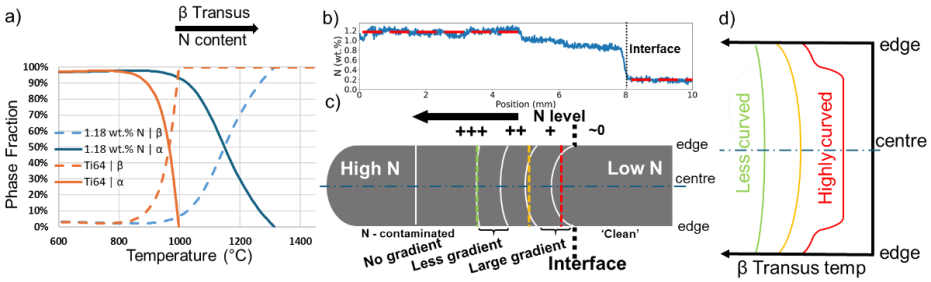


Figure 3. (a) A diagram showing the β-transus temperature of Ti64 (no contaminants) and Ti64 with higher N content (1.18 wt.% as given by EPMA). (b) A line profile of a longer higher spatial resolution EPMA map to show the N content on each part and the gradient along ND. (c) A schematic illustration of the distribution of the N gradients along the ND and (d) a schematic diagram showing T_β profiles relating to HAZ band behaviour.

5. Conclusions

- A higher level of N has an effect of refining of the parent β grains at the outer layer of the WAAM wall.
- Hardness measurements showed an increase in solid solution strengthening by ~25% due to the addition of ~1.2 wt.% N.
- Our results also show that the transformation microstructure is coarsened by 25% in the N-contaminated section.
- The room-temperature transformed microstructure appeared to be affected by the inhomogeneous spatial distribution of the N. The N concentration gradient was suggested to change the position of HAZ bands accordingly due to its influence on the β transus temperature.

Acknowledgements

The authors are appreciative of the EPSRC program grant Sustainable Additive Manufacturing (EP/W01906X/1) for supporting this research. The authors acknowledge the use of equipment within the Advanced Metals Processing and Characterisation themes of the Henry Royce Institute for Advanced Materials, funded through EPSRC grants EP/R00661X/1, EP/S019367/1, EP/P025021/1 and EP/P025498/1.

Reference

[1] Ezugwu E and Wang Z 1997 *J. Mater. Process. Technol.* **68** 262-74
[2] Welsch G, Boyer R and Collings E 1993 *Materials properties handbook: titanium alloys*: ASM international)
[3] Gong G, Ye J, Chi Y, Zhao Z, Wang Z, Xia G, Du X, Tian H, Yu H and Chen C 2021 *J. Mater. Res. Technol.* **15** 855-84
[4] Williams S W, Martina F, Addison A C, Ding J, Pardal G and Colegrove P 2016 *Mater. Sci. Technol.* **32** 641-7
[5] Allen J 2006 *Cost Effective Manufacture via Net-Shape Processing* **17** 1-17
[6] Gardner H, Gopon P, Magazzeni C, Radecka A, Fox K, Rugg D, Wade J, Armstrong D, Moody M and Bagot P 2021 *J. Mater. Res.* 1-16
[7] Ho A, Zhao H, Fellowes J W, Martina F, Davis A E and Prangnell P B 2019 *Acta Mater.* **166** 306-23
[8] Kennedy J, Davis A, Caballero A, White M, Fellowes J, Pickering E and Prangnell P 2021 *Mater. Charact.* **182** 111577
[9] Zhao H, Ho A, Davis A, Antonysamy A and Prangnell P 2019 *Mater. Charact.* **147** 131-45
[10] Keist J S and Palmer T A 2017 *Mater. Sci. Eng., A.* **693** 214-24
[11] Chong Y, Tsuru T, Guo B, Gholizadeh R, Inoue K and Tsuji N 2022 *Acta Mater.* **240** 118356
[12] Issariyapat A, Visuttipitukul P, Umeda J and Kondoh K 2020 *Addit. Manuf.* **36** 101537
[13] Lütjering G and Williams J C 2007 Engineering materials and processes: titanium *New York* 203-50
[14] Caballero A 2023 Effect of different shielding conditions, thermal cycles and post-deposition treatments on melting behaviour and mechanical properties of additively built components. PhD Thesis, Cranfield University
[15] Wriedt H and Murray J 1987 *Bull. Alloy. Phase. Diagr.* **8** 378-88
[16] Davis A, Wainwright J, Sahu V, Dreelan D, Chen X, Ding J, Flint T, Williams S and Prangnell P 2024 *Metall. Mater. Trans. A.* 1-23
[17] Kennedy J R, Davis A E, Caballero A, Williams S, Pickering E and Prangnell P 2021 *Addit. Manuf.* **40** 101928



https://dspace.org/

On the chemical composition, microstructure and mechanical properties of a Nitrogen-contaminated Ti-6Al-4V component built by Wire-Arc Additive Manufacturing

Hu, Dongchen; Biswal, Romali; Sahu, Vivek K.; Fellowes, Jonathan W.; Zadehkabir, A. ...

2024-08-01
IOP Publishing
https://doi.org/10.1088/1757-899x/1310/1/012020
Hu D, Biswal R, Sahu VK, et al., (2024) On the chemical composition, microstructure and mechanical properties of a Nitrogen-contaminated Ti-6Al-4V component built by Wire-Arc Additive Manufacturing. IOP Conference Series: Materials Science and Engineering, Volume 1310, September 2024, Article number 012020

Downloaded from a DSpace repository. https://dspace.org/